King Saud University

Journal of Saudi Chemical Society

www.ksu.edu.sa
www.sciencedirect.com

ORIGINAL ARTICLE

Structural single crystal, thermal analysis and vibrational studies of the new rubidium phosphate tellurate $Rb_2HPO_4RbH_2PO_4 \cdot Te(OH)_6$

Héla Frikha [a],*, **Mohamed Abdelhedi [a]**, **Mohamed Dammak [a]**, **Santiago Garcia-Granda [b]**

[a] *Laboratory of Inorganic Chemistry, Faculty of Sciences University of Sfax, BP 1171, 3000 Sfax, Tunisia*
[b] *Laboratoire de Chimie Physique et Analytique, Faculté de Chimie, Université d'Oviedo, Oviedo 33006, Spain*

Abstract The determination of the crystalline structure of rubidium phosphate tellurate $Rb_2HPO_4RbH_2PO_4 \cdot Te(OH)_6$ [RbPTe] is performed from single crystal X-ray diffraction data. The title compound crystallizes in the monoclinic system P2. The unit cell parameters are as follows: $a = 7.9500(7)$ Å, $b = 6.3085(6)$ Å, $c = 9.5008(9)$ Å, $\beta = 109.783(4)°$, $Z = 2$ and $V = 448.37(7)$ Å^3.

The crystal structure is constituted from isolated (PO_4^{3-}) tetrahedra and (TeO_6^{6-}) octahedra and two nonequivalent Rb$^+$ cations. Material cohesion is built of O–H$\cdots$O bondings and ionic interactions.

The new synthesized material has been characterized using the differential scanning calorimetry (DSC), thermal analysis [differential thermogravimetric analysis (TG), thermodifference analysis (DTA) and the mass spectrometric analysis], FT-IR and Raman techniques.

Thermal analysis, in the temperature range of 300–900 K, confirms that the decomposition of this material took place in two steps. The differential scanning calorimetry analysis shows three endothermic peaks at 451, 463 and 481 K.

The existence of anionic groups in the structure has been confirmed by IR and Raman spectroscopy in the frequency ranges 3000–600 cm^{-1} and 1300–50 cm^{-1}, respectively.

Production and hosting by Elsevier

1. Introduction

In the past decades, an important number of new materials was clearly defined. Many new domains were greatly improved thanks to new phosphate materials. In fact, many inorganic acids such as telluric acid and phosphoric acid have gained attention for their interesting properties like their structural

phase transitions and their associated physical properties: ferroelectricity, electrical relaxation and especially a phase transition into a state characterized by a high protonic conductivity [1–8]. These interesting properties are related to the presence of some anionic groups (TeO$_6^{6-}$, HPO$_4^{2-}$ and (H$_2$PO$_4^-$) in the same unit cell which can favor the presence of the different load centers and to the specific features of hydrogen bonds formed in the crystal structure of these compounds. Therefore, there is great interest to study the family of phosphate tellurate.

A practical point of studying is, that these compounds can be considered as potential proton conductors due to the existence of comparatively strong hydrogen bonds determined by the comparatively strong proton acceptor capabilities of the phosphate, sulfate and arsenate ions [3,4,31].

The influence of cationic substitution on the structural parameters has been reported in previous studies. In fact, while Tl$_2$HPO$_4$TlH$_2$PO$_4$Te(OH)$_6$ [8], Cs$_2$HPO$_4$CsH$_2$PO$_4$Te(OH)$_6$ [9], (NH$_4$)$_2$HPO$_4$(NH$_4$)$_2$H$_2$PO$_4$Te(OH)$_6$ [10] and Na$_2$HPO$_4$-NaH$_2$PO$_4$Te(OH)$_6$ [7] crystallize with the respective space groups, Cm, P2$_1$/m, Pn and P6$_3$22. Whereas, the rubidium phosphate tellurate Rb$_2$HPO$_4$RbH$_2$PO$_4$·Te(OH)$_6$ [RbPTe] exhibits the space group P2$_1$/a [11].

In all cases, the crystal structure determination shows that the main feature of these atomic arrangements is the coexistence of both TeO$_6$ octahedra and PO$_4$ tetrahedra as independent units. The presence of hydrogen atom of PO$_4$ tetrahedra, in this ionic group, can differentiate between this tellurate and other previously studied ones and give new insights on these compounds [1–5].

For all their importance, the recent studies on the phosphate tellurate family still didn't study their physical properties.

Thus, the original aims of the current work are to synthesize and study both crystallographic and physical properties of the title compound Rb$_2$HPO$_4$RbH$_2$PO$_4$·Te(OH)$_6$ [RbPTe]. This led us to study its detailed structure with X-ray crystallography and discuss its behavior during thermal heating.

In the present work, we try to identify the phase transition detected by DSC analysis. DTA/TG analyses allow to determinate the thermal degradation characteristics of rubidium phosphate tellurate during decomposition. Additionally, coupling the DTG apparatus with mass spectrometric analysis makes it possible to identify the type of mass loss during the decomposition. Detailed Raman and vibrational spectroscopy features are given.

2. Experimental and characterizations section

Colorless and transparent single crystals of the rubidium phosphate tellurate Rb$_2$HPO$_4$RbH$_2$PO$_4$·Te(OH)$_6$ [RbPTe] were grown by slow evaporation, at room temperature, from a mixture of telluric acid H$_6$TeO$_6$, rubidium carbonate Rb$_2$CO$_3$ and phosphoric acid H$_3$PO$_4$ in the stoichiometric ratio. The telluric acid and the rubidium carbonate were dissolved in minimum amount of distilled water under stirring up to disparate the powder. After that, we added the phosphoric acid in this aqueous solution. The chemical reaction is as follows:

$$3/2 \text{Rb}_2\text{CO}_3 + 2\text{H}_3\text{PO}_4 + \text{H}_6\text{TeO}_6 \longrightarrow \text{Rb}_2\text{HPO}_4\text{RbH}_2\text{PO}_4 \cdot \text{Te(OH)}_6 + 3/2\text{CO}_2 + 3/2\text{H}_2\text{O}$$

After a few days, colorless and transparent crystals were formed. The product was filtered off with a small amount of distilled water.

A suitable crystal was carefully selected under an optical microscope and selected for X-ray diffraction. Data collection was performed with Kappa CCD APEX II diffractometer Enraf Nonius using Mo Kα radiation (λ = 0.71073 Å) [12].

The chemical purity of the product was tested by EDAX measurements. A semi-quantitative analysis of some crystals extracted from the preparation was performed with a scanning electron microscope.

The structure, Rb$_2$HPO$_4$RbH$_2$PO$_4$Te(OH)$_6$, was analyzed with the crystallographic CRYSTALS program [13]. The structure was solved by conventional Patterson and difference-Fourier techniques.

The Te, Rb and P atoms were refined by Patterson methods and the O and H atom positions were deducted from difference Fourier maps, while H atoms were geometrically placed. The details of data collection and refinement for the title compound are summarized in Table 1. The final positions and equivalent isotropic thermal parameters for the new compound are given in Tables 2 and 3. All drawings were made with the DIAMOND program [14].

The differential scanning calorimetry (DSC) measurements were carried out in a Mettler Toledo DSC model DSC821 with samples placed inside platinum crucibles. In this case, 9.8 mg

Table 1 Main crystallographic, feature X-ray diffraction data parameters results of Rb$_2$HPO$_4$RbH$_2$PO$_4$·Te(OH)$_6$.

Crystal data	
Chemical formula	Rb$_2$HPO$_4$·RbH$_2$PO$_4$·Te(OH)$_6$
Crystal system	Monoclinic
Formula weight	430.23 (g mol^{-1})
Space group	P2
Cell parameters	a = 7.9500(7) Å
	b = 6.3085(6) Å
	c = 9.5008(9) Å
	β = 109.783(4)°
	V = 448.37(7) Å^3
	Z = 2
F(000)	399
Diffractometer	Kappa CCD
Radiation, graphite monochromator	Mo Kα (λ = 0.71073)
θ min/θ max (°)	2.3/27.2°
T (K)	298
ρ_{calc} (g cm^{-3})	3.166
ρ_{min}/ρ_{max}	−1.29(e Å^{-3})/1.57(e Å^{-3})
Index ranges	−7 ⩽ h ⩽ 10
	−8 ⩽ k ⩽ 3, 12 ⩽ l ⩽ 7
Reflections with I > 2σ(I)	1032
Parameters refined	122
Measured reflections	2273
Independent reflections	1073
Goof	1.057
$R_1[F^2 > 2\sigma(F^2)]$	0.047
WR_2 (F^2)	0.052
CCDC deposition number	430865

R = $\sum ||F_o| - |F_c||/\sum|F_o|$ et WR = $(\sum[w(F_o^2 - F_c^2)^2]/[w(F_o^2)^2])^{1/2}$. GooF = S = $\{[w (F^2 - F^2)^2]/(n-p)\}^{1/2}$.

Table 2 Fractional atomic coordinates and equivalent isotropic displacement (U_{iso} for H atoms) for $Rb_2HPO_4RbH_2PO_4 \cdot Te(OH)_6$.

Atoms	x	Y	Z	U_{eq}
Te_1	1.0000	1.01793(9)	1.0000	0.0060
Rb_1	1.0000	1.0009(9)	0.5000	0.0415
Rb_2	0.7567(9)	1.5099(9)	0.7225(9)	0.0581
Rb_3	0.5000	0.0273(10)	1.0000	0.1282
P_1	0.7420(10)	0.4635(10)	1.2830(10)	0.0073
P_2	0.5000	2.0058(10)	0.5000	0.0244
O_1	1.1759(10)	1.2232(10)	1.0256 (10)	0.0139
O_2	1.0699(10)	0.9982(10)	1.2141(10)	0.0130
O_3	1.1806(10)	0.7941(10)	1.0079(10)	0.0186
O_4	0.8616(10)	0.5310(10)	1.1920(10)	0.0185
O_5	0.8487(10)	0.4422(10)	1.4509(10)	0.0282
O_6	0.63690 (10)	0.2651(10)	1.2309(10)	0.0207
O_7	0.6052(10)	0.6408(10)	1.2616(10)	0.0231
O_8	0.5866(10)	2.1397(10)	0.6432(10)	0.0250
O_9	0.6523(10)	2.1612(10)	0.4898(10)	0.0306
H_1	1.2037	1.3522	0.9946	0.0500
H_2	1.1600	0.8867	1.2268	0.0500
H_3	1.3030	0.7470	1.0504	0.0500
H_9	0.7709	2.1829	0.5153	0.0500
H_5	0.8971	0.4551	1.5551	0.0500

$U_{eq} = 1/3 \sum_i \sum_j U_{ij} a_i^* a_j^* a_i a_j.$

Table 3 Anisotropic displacement parameters of $Rb_2HPO_4RbH_2PO_4 \cdot Te(OH)_6$.

Atoms	U_{11}	U_{22}	U_{33}	U_{12}	U_{13}	U_{23}
Te_1	0.0045(7)	0.0120(9)	0.0029(8)	0.0000	0.0031(9)	0.0000
Rb_1	0.0512(7)	0.0301(10)	0.0465(10)	0.0000	0.0208(10)	0.0000
Rb_2	0.0537(7)	0.0627(10)	0.0524(10)	−0.0063(10)	0.0109(10)	0.0137(10)
Rb_3	0.0558(7)	0.2727(10)	0.0556(10)	0.0000	0.0184(10)	0.0000
P_1	0.0069(7)	0.0103(9)	0.0036(10)	0.0013(8)	0.0006(9)	0.0017(10)
P_2	0.0060(7)	0.0541(10)	0.0091(9)	0.0000	−0.0026(9)	0.0000
O_1	0.0160(7)	0.0163(9)	0.0070(10)	−0.0082(8)	0.0010(9)	0.0025(10)
O_2	0.0152(7)	0.0199(10)	0.0033(8)	−0.0003(10)	0.0026(9)	0.0041(9)
O_3	0.0204(7)	0.0176(9)	0.0187(10)	0.0110(8)	0.0080(9)	0.0027(10)
O_4	0.0183(7)	0.0237(10)	0.0183(10)	−0.0025(10)	0.0125(9)	0.0031(10)
O_5	0.0118(7)	0.0650(10)	0.0037(10)	0.0000(10)	−0.0025(10)	−0.0008(10)
O_6	0.0315(7)	0.0161(9)	0.0173(10)	−0.0112(9)	0.0123(10)	−0.0047(10)
O_7	0.0234(7)	0.0240(10)	0.0215(10)	0.0145(9)	0.0071(10)	−0.0051(10)
O_8	0.0113(7)	0.0465(10)	0.0119(9)	0.0030(10)	−0.0026(9)	−0.0000(9)
O_9	0.0147(7)	0.0609(10)	0.0088(10)	−0.0080(9)	−0.0054(9)	0.0045(10)

The anisotropic displacement exponent takes the form: $Exp[-2\pi^2 \sum_i \sum_j U_{ij} h_i h_j a_i a_j^*]$.

of powder sample was thermally treated in the temperature range from 400 K to 550 K at a heating rate of 10 K/min.

A Mettler-Toledo TGA/SDTA851ELF was used for the thermal analysis in oxygen dynamic atmosphere (50 mL/min) at a heating rate of 10 K/min.

The samples, whose masses in TG and DTA measurements were 26.54 mg, were placed inside uncovered alumina crucibles. They were heated from 298 K to 1200 K at a heating rate of 10 K/min.

In the TG test, a Pfeiffer Vacuum ThermoStar™ GSD301 T mass spectrometer was used to determine the evacuated vapors.

Infrared absorption spectrum of the crystalline suspension in KBr was analyzed by a Jasco-FT-IR-420 spectrophotometer in the 3000–600 cm^{-1} frequency range.

Raman spectrum of polycrystalline samples sealed in glass tubes was recorded between 50 and 1300 cm^{-1} in a micro-Raman spectrometer. The Raman spectrum of polycrystalline samples sealed in glass tubes has been recorded on a Labrama HR 800 instrument using 632.81 nm radiations from a physics argon ion laser.

3. Results and discussion

3.1. Scanning electron microscope analysis

The EDAX spectrum of $Rb_2HPO_4RbH_2PO_4 \cdot Te(OH)_6$ reveals the presence of all non-hydrogen atoms: Te, P, Rb and O (Fig 1). Elemental analysis results: for observed atoms, we

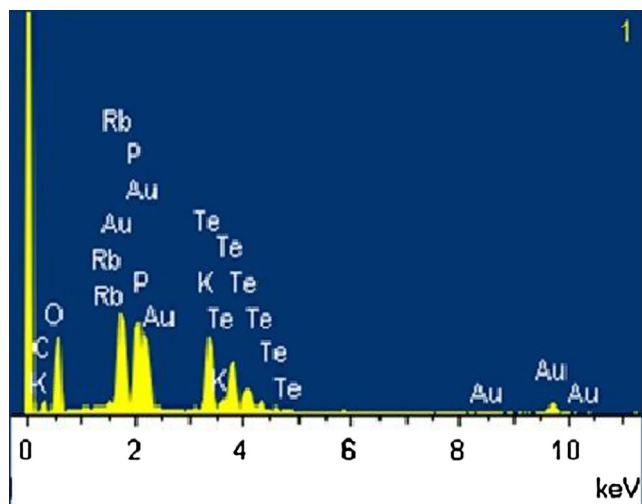**Figure. 1** The EDS spectrum of the $Rb_2HPO_4RbH_2PO_4 \cdot Te(OH)_6$ at room temperature.

have Te: 2.96%, P: 5.92%, Rb: 3.43% and O: 53.63% in close agreement with the composition deducted from the single-crystal X-ray diffraction study.

The scanning electron microscopy (SEM) image shows the morphology of RbPTe crystals in Fig. 2. It can be seen that smaller particles tend to form agglomerates.

3.2. Crystal structure

At room temperature, the structure of $Rb_2HPO_4RbH_2PO_4 \cdot Te(OH)_6$ [RbPTe] is found to be non-centrosymmetric monoclinic $P2$ with unit cell parameters: $a = 7.9500(7)$ Å, $b = 6.3085(6)$ Å, $c = 9.5008(9)$ Å, $\beta = 109.783(4)°$, $Z = 2$, $V = 448.37(7)$ Å³. While the rubidium phosphate tellurate described by Pouchot [11] crystallizes in the monoclinic system with the centrosymmetric space group $P2_1/a$. The unit cell parameters are: $a = 12.261(1)$ Å, $b = 7.059(3)$ Å, $c = 8.225(3)$ Å, $\beta = 90.32(5)°$, $Z = 2$.
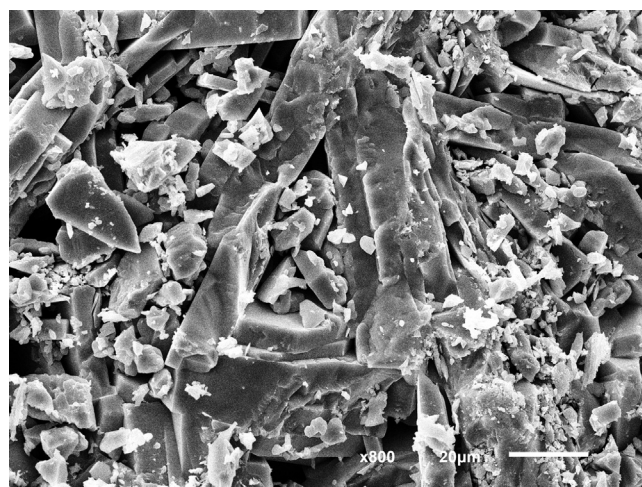
Figure 2 The SEM fracture micrograph of the $Rb_2HPO_4RbH_2PO_4 \cdot Te(OH)_6$.

Fig. 3 shows a projection on the (a, c) plane of the rubidium phosphate tellurate [RbPTe].

The RbPTe structure is built up from $[H_2PO_4]^-$, $[HPO_4]^{2-}$ and TeO_6 polyhedra connected by O–H···O hydrogen bonds (Fig. 4). In consequence, we can notice that the structure is built by cationic and anionic TeO_6–P_1O_4–P_2O_4–P_1O_4–TeO_6 sheets perpendicular to the $\vec{c}$ direction.

3.2.1. Geometry and environment of TeO₆ groups

In the rubidium phosphate tellurate structure, the Te atom occupies a general position.

In fact, the Te–O distances are between 1.860(8) Å and 1.997(8) Å and the O–Te–O angle values vary from 86.59(4)° to 96.86(4)° (Table 4).

However, in the RbPTe described by Pouchot [11], the Te–O distances vary from 1.900(7) Å and 1.921(7) Å with O–Te–O angles are between 87.8(3)° and 92.2(3)°. So, we can notice that these octahedra are more regular.

3.2.2. Geometry and environment of phosphate groups

The asymmetric unit shows two nonequivalent phosphorus sites. The tetrahedral coordination of the P atom is built of four oxygen atoms. The P(1)–O distances in the (RbPTe) structure, vary between 1.4928(9) Å and 1.5467(13) Å with O–P(1)–O angles ranging between 105.62(6)° and 115.18(7)°.

In fact, the second tetrahedron is more deformed than the other tetrahedron. Plus, the PO_4 tetrahedron is made of two P(2)–O distances: 1.5512(8) Å and 1.5861(9) Å and two angles O–P(2)–O: 66.09(5)° and 74.45(4)°. All these values are different from these determined by Pouchot in the rubidium phosphate tellurate described in the recent study where the P–O distances are between 1.513(7) Å and 1.591(7) Å with O–P–O angles between 105.0(4)° and 113.4(4)°. The phosphorus atom, in this structure, occupies only one site.

3.2.3. The rubidium cations environment

The rubidium cation, in the studied RbPTe solid solution, occupies three sites. Eight oxygen atoms coordinate the Rb(1) atoms. The environment of Rb(1) cation is made of four oxygen atoms belonging to P(1)O₄ and two oxygen atoms of second tetrahedral P(2)O₄. The two remaining oxygen atoms belong to the TeO₆ octahedron (Fig. 5). The Rb(1)–O distances are between 2.950(10) Å and 3.555(7) Å.

The Rb(2) cation is coordinated by nine oxygen atoms. Four of them belong to the TeO₆ octahedra, two belong to the P(1)O₄ tetrahedra and three of them belong to the second tetrahedra P(2)O₄ (Fig. 6). The Rb(2)–O distances are between 2.675(9) Å and 3.482(9) Å.

On the other hand, the environment of Rb(3) cation is made up of four atoms belonging to TeO₆ octahedra, two oxygen atoms belonging to P(1)O₄ tetrahedra and two oxygen atoms belonging to second tetrahedra P(2)O₄ (Fig. 7).

The Rb(3)–O distances range is from 2.575(8) to 3.786(9) Å. Table 4 shows the rubidium cation coordination.

On the other hand, the Rb⁺ cation, in the recent study, occupies only two sites and the Rb(1) and Rb(2) cations are coordinated by six and seven oxygen atoms, respectively [11].

In consequence, the high coordination of the rubidium cation in the studied structure explains the stability of this structure due to the high interaction between anionic and cationic groups.
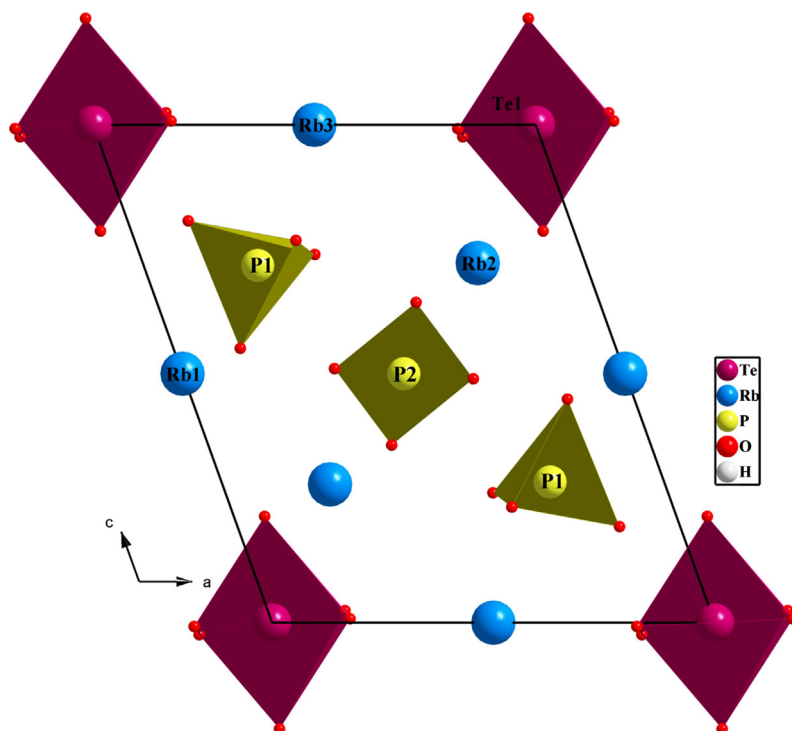
Figure 3   Projection of $Rb_2HPO_4RbH_2PO_4 \cdot Te(OH)_6$ crystal structure in the (a, c) plane.

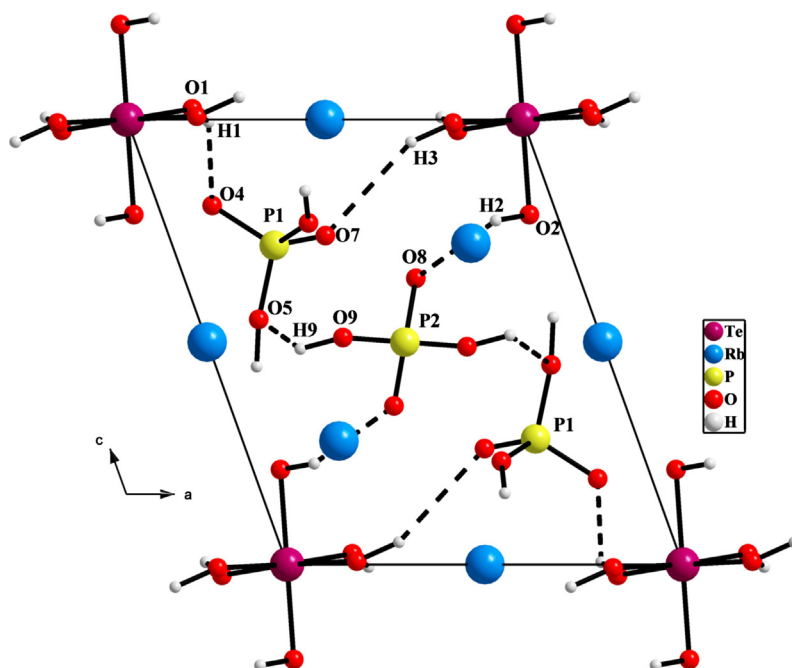**Figure 4**   Projection of RbPTe material crystal on (a, c) plane showing the hydrogen bonds.

3.2.4. The O–H. . .O hydrogen bonds

The strong hydrogen bonds are encountered in both neutral and ionic complexes of acids and bases [15]. The strongest H-bonds in neutral complexes of the O−H· · ·O type are found in dimers of phosphoric and arsenic acids [16–19] and, due to their high thermal stability. On the other hand, the ionic complexes are found to be more stable in the condensed phase [20].

Hydrogen bonds belong to the most important intermolecular bonding phenomena in inorganic solids. Indeed, hydrogen bonds is the bonding interactions between hydrogen atoms and negative charge atoms with (or without) lone pairs [21].

The investigation of the vibrational spectra of hydrogen bonded systems in condensed phases is an important topic in

Table 4 Main inter atomic distances (Å) and bond angles (°) in the RbPTe material.

Phosphate groups

P$_1$–O$_4$ = 1.5467(13)	O$_4$–P$_1$–O$_5$ = 112.11 (6)		
P$_1$–O$_5$ = 1.5392(11)	O$_4$–P$_1$–O$_6$ = 115.18 (7)		
P$_1$–O$_6$ = 1.4928 (9)	O$_5$–P$_1$–O$_6$ = 108.70 (6)	P$_2$–O$_8$ = 1.5512 (8)	O9^{iv}–P2–O8^{iv} = 66.09 (5)
P$_1$–O$_7$ = 1.5249(10)	O$_4$–P$_1$–O$_7$ = 105.62 (6)	P$_2$–O$_9$ = 1.5861 (9)	O9^{iv}–P2–O8 = 74.45 (4)
	O$_5$–P$_1$–O$_7$ = 108.69 (7)	P$_2$–O$_8^{iv}$ = 1.5512 (8)	O8^{iv}–P2–O9 = 74.45 (4)
	O$_6$–P$_1$–O$_7$ = 106.16 (6)	P$_2$–O$_9^{iv}$ = 1.5861(9)	O8–P2–O9 = 66.09 (5)

Tellurate groups

	O$_1$–Te$_1$–O$_2$ = 88.34 (4)
	O$_2$–Te$_1$–O$_3$ = 86.59 (4)
	O$_1^i$–Te$_1$–O$_1$ = 91.82 (5)
	O$_2^i$–Te$_1$–O$_1$ = 96.86 (4)
Te$_1$–O$_1$ = 1.8605(8)	O$_3^i$–Te$_1$–O$_1$ = 89.29 (3)
Te$_1$–O$_1^i$ = 1.8605(8)	O$_2^i$–Te$_1$–O$_1^i$ = 88.34 (4)
Te$_1$–O$_2$ = 1.9235(9)	O$_3^i$–Te$_1$–O$_2^i$ = 86.59 (4)
Te$_1$–O$_2^i$ = 1.9235(9)	O$_3^i$–Te$_1$–O$_2$ = 88.14 (4)
Te$_1$–O$_3$ = 1.9979(8)	O$_1^i$–Te$_1$–O$_2$ = 96.86 (4)
Te$_1$–O$_3^i$ = 1.9979(8)	O$_3^i$–Te$_1$–O$_3$ = 90.04 (5)
	O$_2^i$–Te$_1$–O$_3$ = 88.14 (4)
	O$_1^i$–Te$_1$–O$_3$ = 89.29 (3)

Rubidium groups

Rb$_1$–O$_2$ = 2.9505 (10)	Rb$_2$–O$_1^i$ = 2.9005 (11)	Rb$_3$–O$_1^x$ = 2.9408 (9)
Rb$_1$–O$_2^{vii}$ = 2.9505 (10)	Rb$_2$–O$_2^i$ = 3.4822 (9)	Rb$_3$–O$_1^x$ = 2.9408 (9)
Rb$_1$–O$_5^{iii}$ = 3.0056 (8)	Rb$_2$–O$_2^{viii}$ = 3.3439 (9)	Rb$_3$–O$_3^{iii}$ = 2.9562 (9)
Rb$_1$–O$_5^{iv}$ = 3.0056 (8)	Rb$_2$–O$_3^v$ = 3.0258 (11)	Rb$_3$–O$_3^{iv}$ = 2.9562 (9)
Rb$_1$–O$_9^v$ = 2.9140 (8)	Rb$_2$–O$_4^{iii}$ = 2.8661 (10)	Rb$_3$–O$_6$ = 2.5758 (8)
Rb$_1$–O$_9^{vi}$ = 2.9140 (8)	Rb$_2$–O$_5^{iv}$ = 2.9415 (13)	Rb$_3$–O$_6^{viii}$ = 2.5758 (8)
Rb$_1$–O$_6^{iii}$ = 3.5557 (7)	Rb$_2$–O$_7^{vii}$ = 3.0457 (11)	Rb$_3$–O$_7^{ix}$ = 3.3786 (9)
Rb$_1$–O$_6^{iv}$ = 3.5557 (7)	Rb$_2$–O$_8^v$ = 2.6759 (9)	Rb$_3$–O$_7^v$ = 3.786 (9)
	Rb$_2$–O$_9^v$ = 3.0292 (10)	

Symmetry codes: (i) −x + 2, y, −z + 2; (ii) −x + 1, y, −z + 1; (iii) −x + 2, y + 1, −z + 2; (iv) x, y + 1, z−1; (v) x, y−1, z; (vi) −x + 2, y−1, −z + 1; (vii) x, y, z + 1; (viii) −x + 2, y−1, −z + 2; (ix) −x + 1, y + 1, −z + 2; (x) x + 1, y + 1, z; (xi) −x + 1, y, −z + 2; (xii) −x + 1, y−1, −z + 2.

physics and chemistry. The presence of the hydrogen bond imparts many unusual properties. Indeed, infrared spectroscopy is a very powerful tool for studying H bonded systems. Many results of experimental and theoretical studies of the hydrogen bonds have been studied [22–25].

In fact, infrared spectra of hydrogen-bonded systems are considered as a source of information on the dynamics of weak and medium strength hydrogen bonds.

Over the last several studies, a theoretical of the IR and Raman spectroscopy of hydrogen bond has emerged, which has proven to be useful for interpreting the main features of the hydrogen bond in our phosphate tellurate compound [26].

The PO$_4$ tetrahedra are connected to TeO$_6$ octahedra via O–H···O hydrogen bonds.

The RbPTe structure is stabilized thanks to the hydrogen bonds which link these polyhedral. Indeed they assured the connectivity among the phosphate tetrahedra. We can see that the hydrogen bonds, described in this structure, contribute to form tunnels parallel to $\vec{b}$ direction (Fig. 4).

Consequently, the presence of the hydrogen bonds confirms that the studied material shows interesting physical properties [3,5,27,29,31].

Furthermore, the O···O distances vary from 2.606(6) Å to 3.553(3) Å. In fact, four hydrogen atoms participate in the establishment of the hydrogen bonds (Table 5). So, the hydrogen bonds increase the stability of the new compound. The O···H distances vary from 1.933(5) Å to 2.637(3) Å and O–H···O angles from 139.58(5)° to 156.46(6)°. Those values confirm that the hydrogen bonds are of two types. Strong bonds for O···O distances shorter than 2.7 Å, weaker bonds

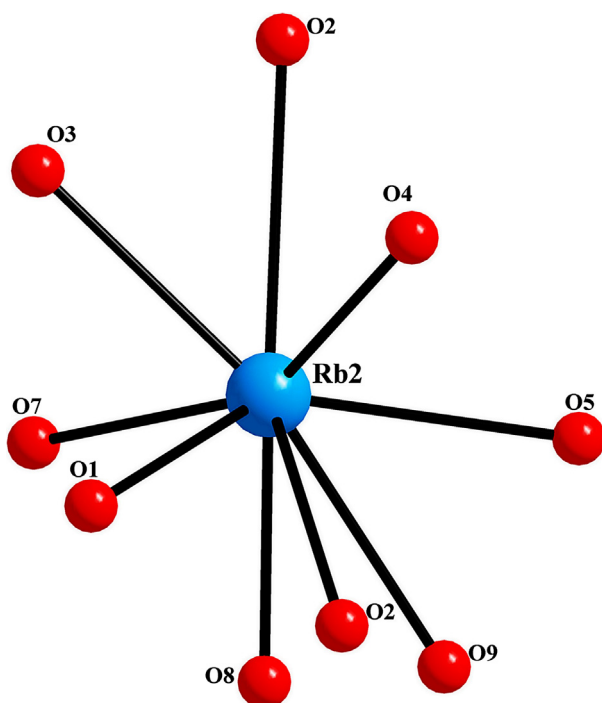**Figure 5** The environment of Rb(1) cation.

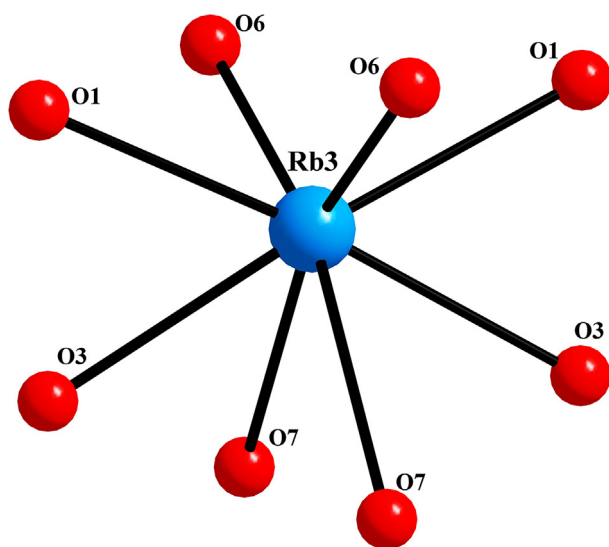**Figure 6**   The environment of Rb(2) cation.

Figure 7   The environment of Rb(3) cation.

Table 5   Geometrical characterization of hydrogen bonds in the RbPTe compound.

D–H$\cdots A$	D–H	H$\cdots A$	$D\cdots A$	D—H$\cdots A$
O_1–$H_1\cdots O_4$	0.918(5)	2.015(3)	2.779(4)	139.58 (5)
O_9–$H_9\cdots O_5$	0.897(3)	1.933(5)	2.606(6)	156.46 (6)
O_2–$H_2\cdots O_8$	0.981(6)	2.015(4)	2.753(10)	145.97(7)
O_3–$H_3\cdots O_7$	0.974(7)	2.637(3)	3.553(3)	149.37(4)

Symmetry codes: (iii) $-x + 2, y + 1, -z + 2$; (xiii) $-x + 2, y, -z + 3$.

for distances of 3.5 Å are formed [20]. The presence of the hydrogen bonds in this material and all these values of $O\cdots O$ and $O\cdots H$ distances explain the origin of interesting physical properties such as the protonic conduction due the breaking of the hydrogen bonds at high temperature.

Our interest in such compounds is supported by the presence of hydrogen atoms in the anionic group. These hydrogen atoms can differentiate between this new structure and other tellurates previously studied and is in agreement with the structural phase transition and superionic conductivity in this material.

3.3. Thermal analysis

The thermal stability of RbPTe was studied in this work to detect the thermal phenomenon. The Fig. 8 shows the DSC curve, while TG/DTG, SDTA curves and the mass spectrometric analysis are depicted in Figs. 9 and 10.
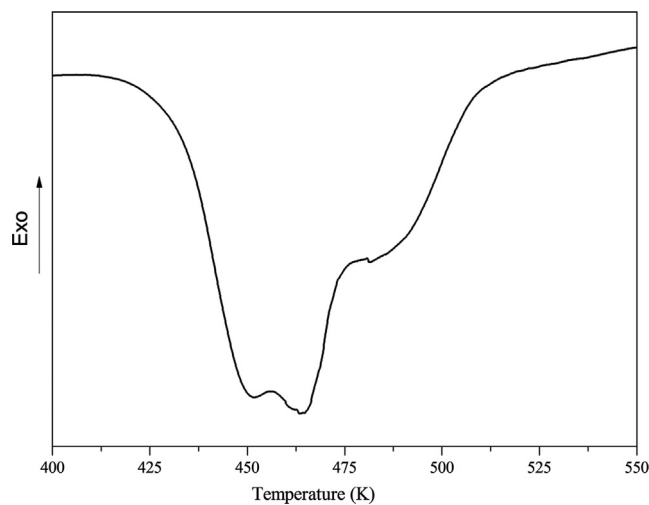

Figure 8   DSC heating curve of $Rb_2HPO_4RbH_2PO_4\cdot Te(OH)_6$ material.
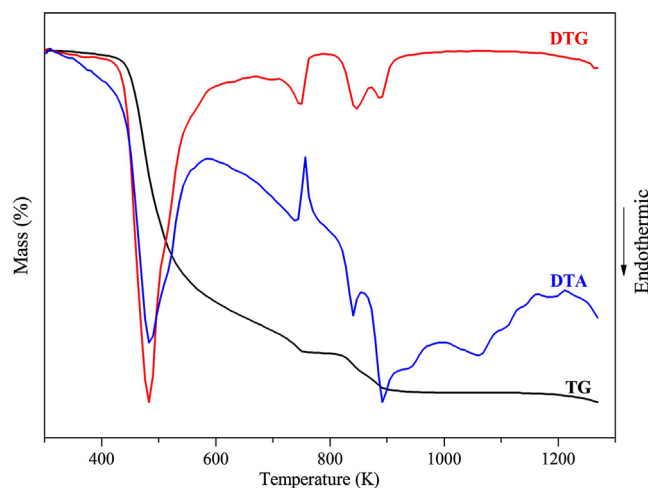

Figure 9   TG–DTG–DTA heating of the $Rb_2HPO_4RbH_2PO_4\cdot Te(OH)_6$ compound.
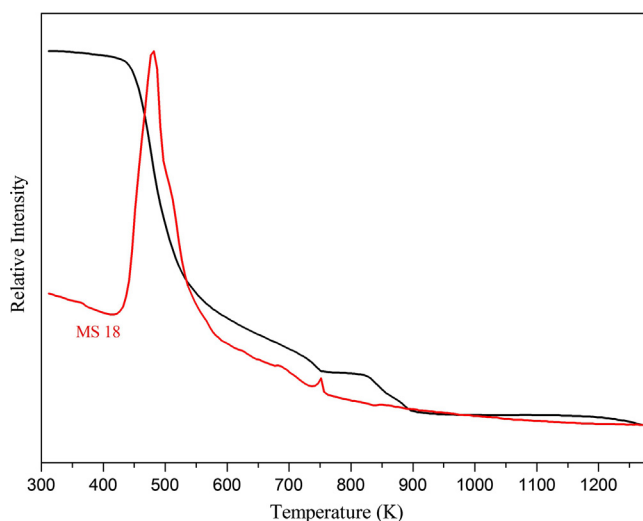
Figure 10 MS signals of evacuated vapors on the TG experiment for RbPTe material m/z 18/H$_2$O.

The DSC (Fig. 8) presents a result of the calorimetric study, showing the obtained diagram on heating from 400 K to 550 K of the titled compound. The DSC curve reveals three endothermal peaks at 451, 463 and 481 K. By comparison with similar materials, the first at 451 K can be due to a ferroelectric-paraelectric phase transition and the second at 463 K can be attributed to a ionic protonic conduction phase transition, whereas the third at 481 K accompanied with the mass loss can be attributed to the beginning of the decomposition of the material [3,27–30].

In previous studies, only the structural studies of the rubidium phosphate tellurate has been described. In this context, it was interesting to study the thermal behavior of this compound.

TG/DTG curves of RbPTe reveal total mass losses after 430 K of respectively, 15%, from 300 to 1000 K. The mass loss of Rb$_2$HPO$_4$RbH$_2$PO$_4$·Te(OH)$_6$ proceeds by two separate and defined steps.

The first step between 430 and 751 K (which reaches its maximum velocity at 482 K), the mass loss of 12%, associated with endothermic peak at 484 and 481 K on the DTA and DSC curves, respectively. There is one maximum peak in MS 18 at 481 K which overlaps with endothermic peak on DTA at 484 K, which indicates the dehydration process.

The dehydration process, corresponds to the loss of three water molecules (calculated weight loss 12%): resulting from the decomposition of telluric acid Te(OH)$_6$ as the following equation:

$$Te(OH)_6 \rightarrow TeO_3 + 3H_2O$$
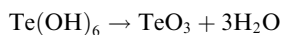
Comparing the obtained results with the already made studies, we can notice that the decomposition of telluric acid is not a single-step process [31].

The thermal transformation of the telluric acid shows the intermediate product, such as the orthotelluric acid.

$$Te(OH)_6 \rightarrow H_2TeO_4 + 2H_2O$$
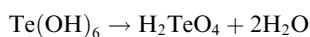
Moreover, in the temperature range of 550–715 K the orthotelluric acid H$_2$TeO$_4$ begins to decompose with the water liberation [32].

$$H_2TeO_4 \rightarrow TeO_3 + H_2O$$
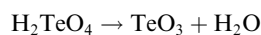
The second step, 750 and 900 K, which reaches its maximum velocity at 751 K, the mass loss of 3%, is associated with endothermic peak on the DTA at 891 K corresponding to the loss of one water molecule. Furthermore, the hydrogen phosphate H$_2$PO$_4$ acid decomposes to liberate the water and gives PO$_3$ [33,34].

$$H_2PO_4 \rightarrow PO_3 + H_2O$$
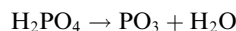
3.4. Vibrational studies

In the present work, the vibrational spectroscopy of Rb$_2$HPO$_4$RbH$_2$PO$_4$·Te(OH)$_6$ has been studied to define the symmetry of the anions and to elucidate the distribution of energy levels in their crystal lattices.

The spectroscopy characteristics of the HPO$_4^{2-}$ ion with pseudo-symmetry C$_{3V}$ can be determined by the free tetrahedral PO$_4^{3-}$ entity. In order to confirm the existence of the two anions PO$_4^{3-}$ and TeO$_6^{6-}$ and to study the presence and the characteristics of the hydrogen bonds in their crystal lattice, IR and Raman spectroscopic studies of Rb$_2$HPO$_4$RbH$_2$PO$_4$·Te(OH)$_6$ have been performed in the frequency range (4000–600) cm^{-1} and (50–1300 cm^{-1}), respectively. Vibrational spectroscopy offers valuable complementary insight into the dynamics of hydrogen bond.

The observed IR and Raman spectra of the RbPTe compound are plotted in respectively (Figs. 11, 12a and 12b). The peaks positions and their assignment to different modes for RbPTe are provided in Table 6.

Consequently, the vibrational spectra are expected to differ in frequency values and intensities depending on the symmetry. To make a qualitative assignment of the Raman and IR peaks to vibrational modes, we examine the modes and frequencies observed in similar phosphate compounds. The vibrational modes are similar to those reported earlier for phosphate tellurate [35].

The IR and Raman spectra of RbPTe, consist of a number of distinct separated groups that can be divided into three fre-
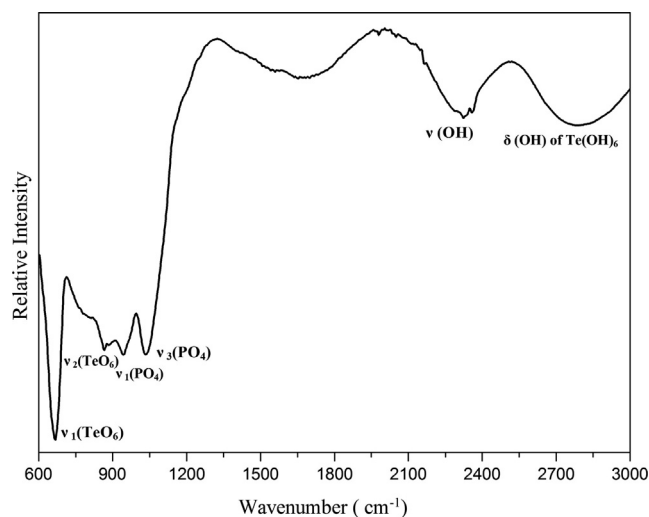

Figure 11 IR spectrum of Rb$_2$HPO$_4$RbH$_2$PO$_4$·Te(OH)$_6$ material at room temperature.
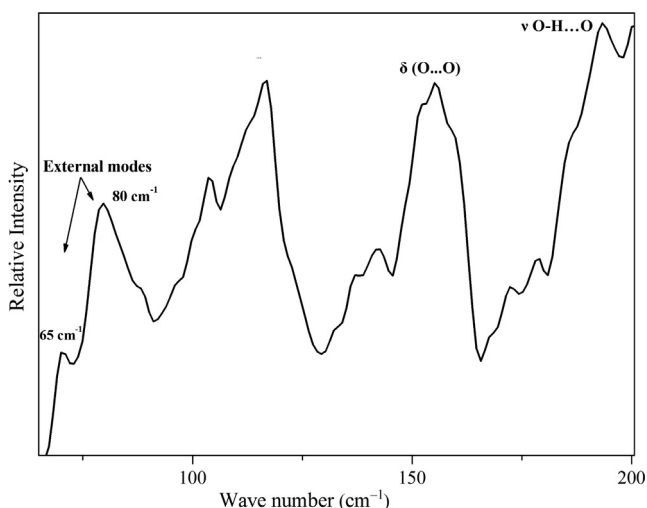
Figure 12a   Raman spectra, in frequency range 50–200 cm^{-1}, of the Rb$_2$HPO$_4$RbH$_2$PO$_4$·Te(OH)$_6$ compound.
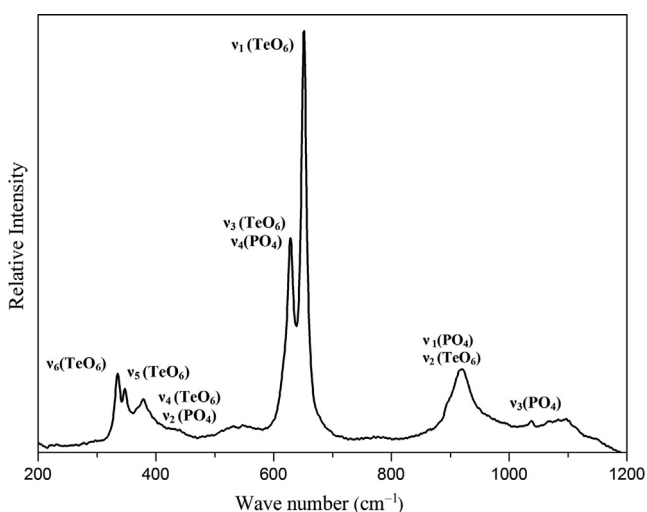
Figure 12b   Raman spectra, in frequency range 200–1200 cm^{-1}, of the Rb$_2$HPO$_4$RbH$_2$PO$_4$·Te(OH)$_6$ compound.

quency regions: 15–250 cm^{-1} for lattice mode, 250–1200 cm^{-1} for PO$_4^{3-}$ internal modes and 1200–3700 cm^{-1} for high frequency hydrogen modes [36,37].

The vibrations analysis of the orthophosphate tetrahedron shows that this group has four vibrational frequencies, two stretching modes v_1 and v_3 (respectively, symmetric and asymmetric), and two bending modes v_2 and v_4 [38].

3.4.1. Interpretation of IR spectrum

The infrared spectroscopy is an important method to understand the physical informations on the dynamics of hydrogen bonds. This spectroscopy has been the object of considerable experimental and theoretical works in the literature [25,26].

In FT-IR spectrum the bands are formed by bending and stretching vibrations of Te/P–O bonds in the phosphate tellurate material.

Table 6   Infrared and Raman frequencies and their assignments for Rb$_2$HPO$_4$RbH$_2$PO$_4$·Te(OH)$_6$.

IR (cm^{-1})	Raman (cm^{-1})	Assignment	
2783 w		δ(OH) of Te(OH)$_6$	
2358 vw			
2328 vw		v(OH) of strong	
2049 w		hydrogen bond(Te/P–O)	
1671 m			
1033 m	1037 vw	v_3(PO$_4$)	
943 w	918 m	v_1(PO$_4$)	
864 w		v_2(TeO$_6$)	
666 s	652 vs	v_1(TeO$_6$)	
	627 m	v_3(TeO$_6$) and v_4(PO$_4$)	
	378 m	v_4(TeO$_6$) and v_2(PO$_4$)	
	347 vw	v_5(TeO$_6$)	
	333 w	v_6(TeO$_6$)	
	193 vw	v O–H$\cdots$O	
	155 vw	δ(O$\cdots$O)	
	116 vw		
	80 vw	External modes	
	65 vw		

Relative intensities: vs: very strong; s: strong; m: medium; w: weak; sh: shoulder; vw: very weak.

The bands at 666 cm^{-1} and 864 cm^{-1} are attributed, respectively to v_1(TeO$_6$) and v_2(TeO$_6$) [39].

The peaks observed at 943 cm^{-1} and 1033 cm^{-1} are assigned respectively to the v_1(PO$_4$) and v_3(PO$_4$).

The (Te)O–H and (P)O–H stretching vibrations are expected in the region 2300–3900 cm^{-1}. This high value for P–O(H) stretching vibration indicates that the hydrogen is lightly bonded to the oxygen atom [40].

In fact, these peaks which appear at 1671 cm^{-1}, 2328 cm^{-1} and 2783 cm^{-1} are attributed to δ(O–H$\cdots$O).

3.4.2. Interpretation of Raman spectrum

At room temperature, the Raman spectrum of the Rb$_2$HPO$_4$RbH$_2$PO$_4$·Te(OH)$_6$ material was studied. According to the Raman spectra of the other phosphate, the most intense peak observed at 652 cm^{-1}, was assigned to v_5(TeO$_6$), while the less intense peak, at 627 cm^{-1}, was assigned to modes v_3(TeO$_6$) and v_4(PO$_4^{3-}$).

Moreover, the vibration v_4(TeO$_6$) appears with v_2(PO$_4^{3-}$) at 378 cm^{-1}, the peak attributed to v_5(TeO$_6$) is found at 347 cm^{-1} and the vibration v_6(TeO$_6$) appears at 333 cm^{-1}.

In the Raman spectra, the symmetric stretching mode v_1(PO$_4^{3-}$) and asymmetric stretching mode v_3(PO$_4^{3-}$) occurred at respectively 918 cm^{-1} and 1037 cm^{-1} [41].

The very weak line at 193 cm^{-1} is assigned to the motion of the O–H$\cdots$O hydrogen stretching, while the lattice modes observed at the low-frequency with a very weak band at 155 cm^{-1} and 116 cm^{-1}.

The peak located at 80 cm^{-1} is attributed to δ(O$\cdots$O), whereas, the translational vibrations of Rb$^+$ ions appear at 65 cm^{-1} [42].

All peaks are well resolved, however the ordered state of the structure and the presence of all the vibration modes show the existence of all molecular groups.

4. Conclusion

In this work, we have synthesized the $Rb_2HPO_4RbH_2PO_4 \cdot Te(OH)_6$ by slow evaporation technique. The rubidium phosphate tellurate RbPTe structure has been determined on a single crystal. The studied phosphate tellurate material crystallizes in the monoclinic system with non-centrosymmetric $P2$ space group.

Besides that, the DSC curve shows a phase transition before the decomposition confirmed by DTA.

According to MS analysis, the decomposition was followed by the release of H_2O. The multi-step thermal decomposition process was observed for rubidium phosphate tellurate with the release of H_2O that came from the decomposition of hydrogen phosphate H_2PO_4 and $Te(OH)_6$ acids. Thus, the couple of DTA/TG with mass spectrometry is a very useful tool for analyzing the thermal decomposition of the phosphate tellurate family.

Indeed, the vibrational study which has been resulted at room temperature, confirms the presence of (PO_4^{3-}) tetrahedra and (TeO_6^{6-}) octahedra linked with $O-H\cdots O$ hydrogen bond which can be the source of interesting physical properties.

Acknowledgments

References

[1] R. Zilber, A. Durif, M.T. Averbuch-Pouchot, Acta Cryst. B37 (1981) 650.
[2] R. Zilber, A. Durif, M.T. Averbuch-Pouchot, Acta Cryst. B38 (1982) 1554.
[3] M. Dammak, H. Khemakhem, T. Mhiri, J. Phys. Chem. Solids 62 (2001) 2069.
[4] N. Chabchoub, H. Khemakhem, M. Gargouri, J. Alloys Compd. 359 (2003) 84.
[5] M. Abdelhedi, M. Dammak, A. Cousson, A.W. Kolsi, J. Alloys Compd. 398 (2005) 55.
[6] A. Durif, M.T. Averbuch-Pouchot, J.C. Guitel, Acta Cryst. B35 (1979) 1444.
[7] M.T. Averbuch-Pouchot, Acta Cryst. B36 (1980) 2405.
[8] M.T. Averbuch-Pouchot, A. Durif, Mater. Res. Bull. 16 (1981) 71.
[9] M.T. Averbuch-Pouchot, A. Durif, J.C. Guitel, Mater. Res. Bull. 15 (1980) 387.
[10] T. Kikuta, D. Hamatake, T. Yamazaki, N. Nakatani, J. Korean Phys. Soc. 46 (2005) 211.
[11] M.T. Averbuch-Pouchout, A. Durif, J.C. Guitel, Mater. Res. Bull. 14 (1979) 1219.
[12] Nonius, Kappa CCD Sever Software, Nonius, B.V. Delft, The Netherlands, 1997.
[13] P.W. Betteridge, J.R. Carruthers, R.I. Cooper, K. Watkin, J. Appl. Cryst. 36 (2003) 1487.
[14] K. Brandenburg, M. Berndt, DIAMOND. Version 2.1.b, Crystal impact Gb R, 1999, Bonn, Germany.
[15] E. Grech, Z. Malarski, W. Sawka-Dobrowolska, L. Sobczyk, J. Mol. Struct. 416 (1997) 227.
[16] L.C. Thomas, R.A. Chittenden, H.E. Hartley, Nature 192 (1961) 1283.
[17] J.A. Walmsley, J. Phys. Chem. 88 (1984) 1226.
[18] S. Detoni, D. Hadzi, Spectrochim. Acta 20 (1964) 955.
[19] H.D. Lutz, B. Engelen, Trends Appl. Spectrosc. 4 (2002) 355.
[20] A. Novak, Hydrogen Bonding in Solids, Spring-Verlag, Berlin, Heidelberg New York, 1974, p. 177, 18.
[21] H.D. Lutz, J. Mol. Struct. 646 (2003) 227.
[22] N. Rekik, H. Ghalla, H.T. Flakus, M. Jablonska, B. Oujia, J. Comput. Chem. 31 (2009) 3.
[23] N. Rekik, H.T. Flakus, A. Jarczyk-Jędryka, F. Abdulaziz-Agel, M. Daouahi, P.G. Jones, J. Kusze, M. Nowak, J. Phys. Chem. Solids 77 (2015) 68.
[24] N. Rekik, Phys. B 4 (36) (2014) 164.
[25] N. Rekik, H. Ghalla, G. Hanna, J. Phys. Chem. 116 (2012) 4495.
[26] A. Hadrich, A. Lautie, T. Mhiri, F. Romain, Vib. Spectrosc. 26 (2001) 51.
[27] K. Ghorbel, H. Litaiem, L. Ktari, S. Garcia-Granda, M. Dammak, Ionics 22 (2016) 251.
[28] H. Derbel, S. Kamoun, F. Hlel, M. Gargouri, Phys. Sci. 1 (2011) 1.
[29] M. Djemel, M. Abdelhedi, M. Dammak, A.W. Kolsi, J. Mol. Struct. 1033 (2013) 84.
[30] S. Guillot Gauthier, J.C. Peuzin, M. Olivier, G. Rolland, Ferroelectrics 52 (1984) 293.
[31] I. Bechibani, H. Litaiem, L. Ktari, J. Lhoste, M. Dammak, J. Mol. Struct. 1045 (2013) 199.
[32] J. Faby, J. Loub, L. Feltl, J. Therm. Anal. 24 (1982) 95.
[33] B. Bazan, J.L. Mesa, J.L. Pizarro, L. Lezama, A. Pena, M.L. Arriortua, T. Roja, J. Solid State Chem. 179 (2006) 1459.
[34] S. Ekambaram, S.C. Sevov, Inorg. Chem. 39 (2000) 2405.
[35] D. Philip, G. Aruldhas, J. Raman Spectrosc. 29 (1989) 637.
[36] N.L. Calve, F. Romain, M.H. Limage, A. Novak, J. Mol. Struct. 200 (1989) 131.
[37] F. Romain, A. Novak, J. Mol. Struct. 263 (1991) 69.
[38] A.C. Chapman, D.A. Long, D.T.L. Jones, Spectrochim. Acta 21 (1965) 633.
[39] D. Philip, D. Abraham, G. Aruldhas, J. Raman Spectrosc. 21 (1990) 521.
[40] J. Gaumt, Trans. Faraday Soc. 49 (1953) 112.
[41] H. Naili, T. Mhiri, A. Daoud, Phase Transitions 71 (1999) 271.
[42] H. Naïli, L. Vendier, J. Jaud, T. Mhiri, Solid State Sci. 3 (2001) 677.